Progress In Electromagnetics Research, Vol. 111, 91–104, 2011

EXPERIMENTAL STUDY ON A FLANGED PARALLEL-PLATE DIELECTRIC WAVEGUIDE PROBE FOR DETECTION OF BURIED INCLUSIONS

H. Zhang, S. Y. Tan, and H. S. Tan

School of Electrical and Electronic Engineering
Nanyang Technological University, Singapore 639798, Singapore

Abstract—This paper presents an experimental study of a flanged parallel-plate dielectric waveguide (PPDW) probe for detecting dielectric inclusions in a dielectric host medium, with different electrical properties from the inclusions. The S-parameter signals from an inclusion (modelled as a conducting sphere) are shown to have resonant characteristics, from which the size and location of the inclusion can be deduced. As an example of a possible application for this technique, we use parameters of host medium and inclusions relevant for detection of tumors in body tissues. An experimental study was performed on solid tissue-simulating phantoms with embedded conducting dielectric inclusions. The measurements show promising results.

1. INTRODUCTION

Microwave characterization and detection of hidden or partially obscured targets, in studies such as demining or radar target recognition [1–4], through-wall imaging for fire-rescue operations and other emergency reliefs [5–7], pipeline localization [8], botanical applications [9–11] have received considerable attention recently, especially in the development for nondestructive and non-invasive imaging systems such as biomedical diagnostics [12–16] and detection of contaminants in food products [17].

In earlier papers, we have proposed a flanged parallel-plate dielectric waveguide probe (PPDW) [18, 19], for the detection and localization of small spherical objects embedded in a lossy dielectric medium. The principle of this technique is based on detecting

Received 7 November 2010, Accepted 24 November 2010, Scheduled 30 November 2010
Corresponding author: Soon Yim Tan (esytan@ntu.edu.sg).

the significant dielectric contrast between the inclusion and the host medium. The PPDW is used to make contact S parameter measurements at the interface with the medium. An inclusion having a complex permittivity significantly higher than that of the host medium alters the S_{11} at the aperture of the PPDW, and the S_{11} displays resonant characteristics over the swept frequencies. The greater this dielectric contrast between the inclusion and the host medium, the greater the resonant backscattered signals. Hence this magnitude can be used to differentiate the inclusion from other clutter items which have lower contrast dielectric properties than the inclusion. The size of the inclusion can be estimated from the resonant frequency of the S_{11}. In addition, the localization of the inclusion can be achieved with S_{21} measurements with the use of a triangulation technique in which several PPDW are used.

In this paper, experimental validations of this technique to detect and estimate the size of buried inclusion are presented. The studies were performed on solid lossy dielectrics which were fabricated in our laboratory together with embedded conducting spherical inclusions. Possible applications for our PPDW technique are in the food industry to detect plastics and metal objects in media such as dry powdered food and grains where the contaminants, have significantly large dielectric contrast from the host medium.

2. REVIEW OF THEORETICAL FORMULATION

The basis of the detection of the buried objects using PPDW is the Mie scattering of spherical bodies [20]. The PPDW acts as the microwave source radiating into the embedding medium. It is assumed that the incident field on the small spherical inclusion embedded in the medium is locally plane, and the scattered electric field into the aperture of the PPDW is also a plane wave. For a plane wave propagating with wavenumber k_2 in the negative z_1'-direction, with amplitude E_o, polarized in the x_1'-direction propagating as shown in Fig. 1, the scattered electric field at a point $P(r_1', \theta_1', \phi_1')$ outside the sphere can be expressed as [20]

$$E^s(P) = E_o \frac{e^{ik_2 r_1'}}{k_2 r_1'} [\cos\phi_1' S_1(\theta_1') \hat{a}_{\theta_1'} - \sin\phi_1' S_2(\theta_1') \hat{a}_{\theta_1'}] \qquad (1)$$

where $S_1(\theta_1')$ and $S_2(\theta_1')$ are the complex amplitudes of the scattered radiation in the θ_1' and ϕ_1' polarization directions. The detailed expressions of these coefficients involved in the equation are given in [19]. Using uniform geometrical theory of diffraction (UTD), a field point (x_0, z_0) in Region II is illuminated by the fields diffracted

from the two wedges at the flanges of the PPDW at W_1 and W_2 (see Fig. 1) [21, 22]. Resolving the incident fields $E_x^{II}(x_0, z_0)$ and $E_z^{II}(x_0, z_0)$ on the inclusion in the directions from W_1 and W_2 (i.e., $\hat{a}_{kt1}$ and $\hat{a}_{kt2}$) results in two contributions of scattered field $E_1^s(r'_1, \theta'_1, \phi)$ and $E_2^s(r'_2, \theta'_2, \phi)$. The superposition gives the effective scattered signal E^s.

With reference to Fig. 1, the backscattered signal in S_{11} and scattered signal in S_{21} in the presence of an inclusion can thus be found respectively to be

$$S_{11} = \Gamma_0 + \Delta\Gamma \tag{2}$$

$$S_{21} = \Delta\Gamma \tag{3}$$

where

$$\Delta\Gamma = \frac{\tau_0 \left[E_1^s(r'_1 = r_0, \theta'_1, \phi) + E_2^s(r'_2 = r_0, \theta'_2, \phi)\right]}{E_x^i} \tag{4}$$

Γ_0 is the reflection coefficient due to discontinuities of the media (interface between the detector and embedding medium) in the absence of any inclusion; E_x^i denotes the incident field at the aperture; the probe receiving characteristic τ_0 is dependent on angle θ_i. It is assumed that the transmitting and receiving PPDWs are in the same plane. Detailed derivations can be found in [19].

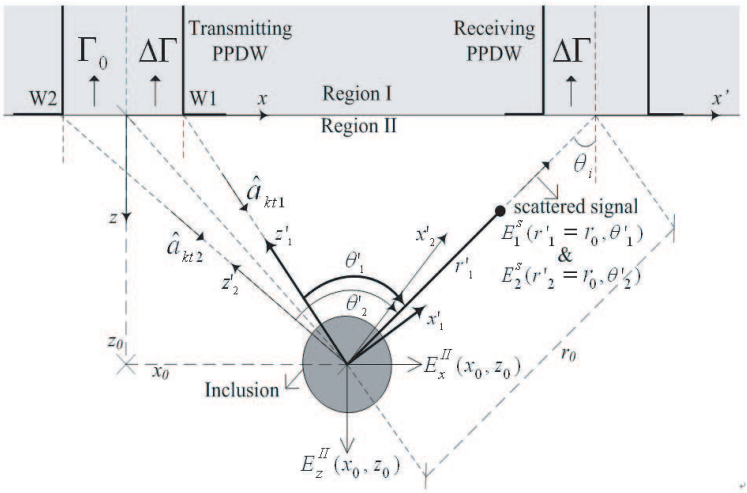

Figure 1. PPDW is illuminating the inclusion for S_{11} measurement; another PPDW is measuring S_{21}.

3. METHODOLOGY

By making N contact measurements at various positions of the medium under study, ${}^{N}C_2$ pairs of ΔS_{11} (difference in S_{11}) are obtained. It is to be noted one of the issues in detecting embedded obstacles using microwave techniques is the interface between the detector and the medium, and ensuring that the interface scattering does not obscure the reflections from the target. Hence in this method, by performing differential measurements, the interface scattering (the term Γ_0 in (2)) is eliminated.

Over the swept frequencies, the resonant ΔS_{11} with respect to amplitude refers to one of the pair of S_{11} measurements which contains the backscattered signal from the inclusion, $\Delta\Gamma$. An absence of any resonant behavior indicates that no inclusion is present at the positions where the pair of measurements is made. Eliminating the positions that yield such non-resonant ΔS_{11}, the region having an embedded inclusion can thus be identified. Subsequently the PPDW can scan around this region for maximum resonating response of ΔS_{11} since the inclusion would be closest to the final position that yields this ΔS_{11} with resonant characteristics. The resonant frequency(ies) of this maximum resonant ΔS_{11} contributed by the inclusion can be used to estimate its size. The magnitude of the resonant backscattered signals may be used to differentiate between the targeted inclusion having dielectric contrast of about 8 times or more from the embedding medium. To locate the depth of embedment, with a PPDW transmitting at a given position, another PPDW scans for minimum S_{21}. Typically the scattered signal is weakest at right angles to the direction of propagation of the incident field. The positions of the transmitting PPDW, the PPDW receiving minimum S_{21} and the inclusion would form a right-angled triangle where a simple triangulation technique can be used to determine the depth of embedment.

4. EXPERIMENTAL RESULTS AND DISCUSSIONS

4.1. Solid Phantom and Inclusion

In our experimental studies of the PPDW, we use as the host lossy dielectric medium, an oil-in-gelatine dispersion formulation used in [23, 24] that can produce a wide range of dispersive dielectric properties simply by varying the concentration of oil used. The detailed procedure for the fabrication of this dielectric material can be found in these literatures. We vary recipe in [23] to facilitate the procurement of local ingredients by using deionised (DI) water (Nam

Wah Battery, Singapore), 160 gelatine powder, and surfactant 'Ligent' dishwashing detergent (Yuri Distribution Co., Singapore). It is shown in Fig. 2 the dielectric constant and loss tangent of phantom samples with varying percentages of oil, measured using an Agilent high temperature dielectric probe 85070E, seven days after preparation. As the percentage of oil increases in the emulsion, the dielectric constant and the loss tangent both decrease.

It is used in the experiments, the embedding dielectric medium fabricated with 80% oil-concentration emulsion. Furthermore, we use inclusions in the embedding dielectric having diameters from 8 to 16 mm. Dielectric spheres made from 10% and 70% oil-concentration emulsion are also used, to simulate an approximately 8 times,

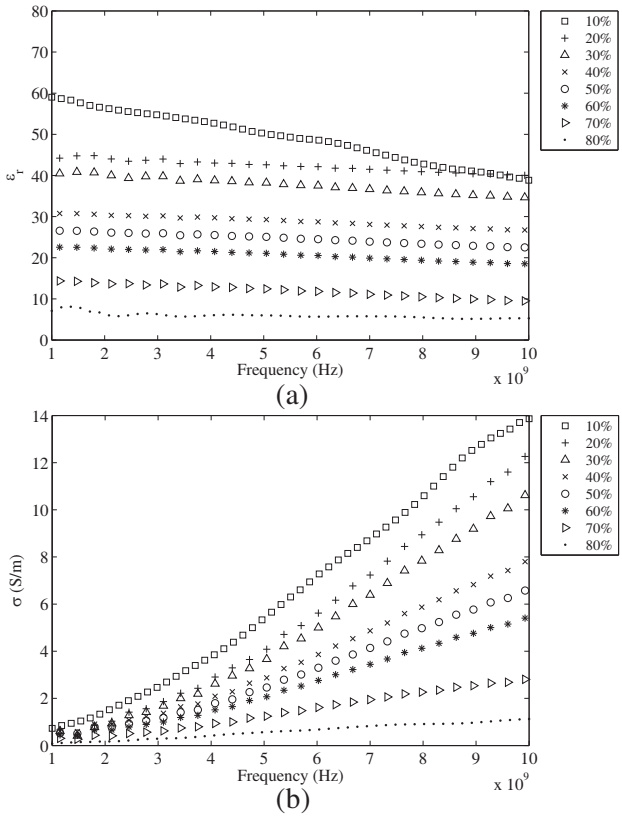

Figure 2. (a) Dielectric constant and (b) loss tangent of phantom samples with varying percentages of oil, measured 7 days after preparation.

and 2 times dielectric variability in dielectric properties respectively between the targeted inclusion and the embedding medium. Spherical inclusions are used as an example to validate the theoretical predictions based on the Mie. Theory, although this proposed PPDW and technique is not restricted to the detection of spherical bodies. Each inclusion is mounted on top of a plastic plug at the base of a mould, with a 2 mm diameter wooden stick to simulate a depth of embedment, h (calculated from the surface of the embedding dielectric to the centre of the inclusion).

Separate embedding dielectrics were fabricated to simulate the different-scenario studies. In addition to obtaining the ease of fabrication, this method introduces variability and uncertainty in the dielectric properties which will provide a realistic platform to model the inhomogeneous nature of some embedding media.

4.2. Prototype and Measurement Setup

The geometry of the prototype is given in Fig. 3. A detailed description of the design of parameters of the central dielectric guide (ECCSTOCK® Hik500F, $k = 10$) for dominant TE_{10} mode propagation can be found in [25]. Teflon screws and spacers are used at the sides of the flanged copper plates to maintain uniform spacing between them and to secure the central dielectric guide and the copper short in their positions.

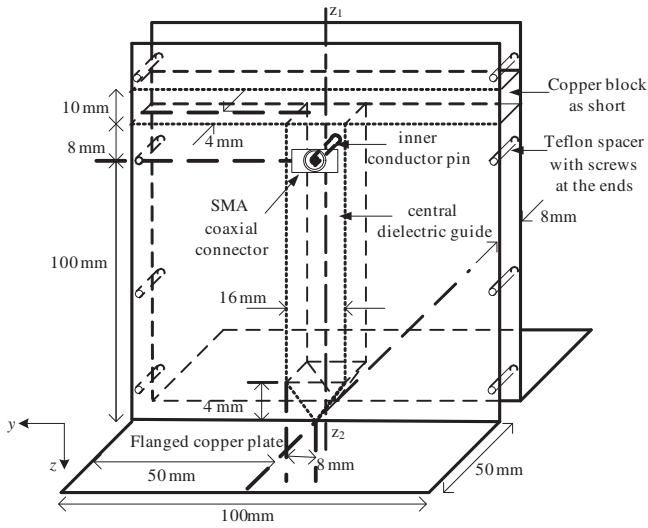

Figure 3. Geometry of the prototype PPDW fabricated.

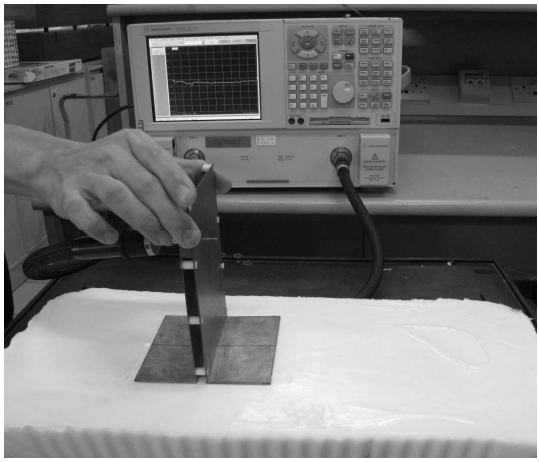

Figure 4. Experimental setup.

S parameters measured by the PPDW are recorded with an Agilent PNA-L Network Analyzer N5230A connected to a 50 Ω coaxial cable; and the measurement system is set up as shown in Fig. 4. The PPDW axis and the spherical inclusion are aligned along positioned along $z_1 z_2$, (see Fig. 3) to enable the maximum backscattered signals from the inclusions to be measured. The PPDW is hand-held and rests on the phantom surface during the measurements. Once the probe is calibrated, there is no need for further calibrations when performing measurements at different positions of the phantom.

4.3. Results and Discussions

4.3.1. Identify Presence

Three measurements of S_{11} are made on a lossy dielectric without any inclusions (D_1), giving three ($^3C_2$) ΔS_{11} values. These three values are almost identical and are shown in Fig. 5 as one representative ΔS_{11}. As observed, the ΔS_{11} response in the absence of any inclusions is very small, on average lower than −50 dB. The embedding host dielectric medium is fabricated in our lab and inevitably has small inhomogeneities due to uneven stirring. Fig. 5 also shows the magnitude of ΔS_{11} obtained from the measurements made on different host dielectrics containing respectively a metal and dielectric inclusion of 8 mm diameter embedded at the same depth $h = 2$ cm; and one of arbitrarily chosen S_{11} recorded on D_1 (embedding dielectric without inclusion). It is observed that the average resonant backscattered amplitude from the metal inclusion and the dielectric inclusion having

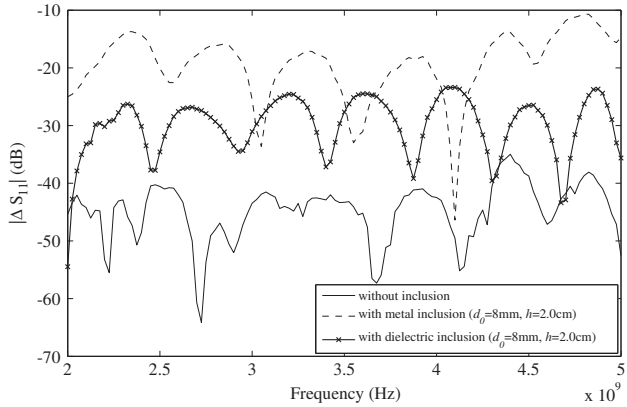

Figure 5. Magnitude of ΔS_{11} for phantom without inclusion; and with metal and dielectric inclusions of 8 mm diameter, embedded at a depth of 2 cm.

dielectric contrast of about 8 times compared with the embedding medium, is about 25 dB and 15 dB respectively higher than any of the ΔS_{11} obtained earlier that represents scattering due to medium inhomogeneities (the exact values are dependent on each phantom fabricated).

4.3.2. Estimate Size

It is possible to estimate the size of an inclusion from the calibrated resonant frequencies f_r of the ΔS_{11}, as f_r depends on the size and is independent of the depth of embedment h in the medium [18]. Fig. 6 shows the normalized ΔS_{11} for inclusions of different diameters, $d_0 = 8\,\text{mm}$, 12 mm, and 16 mm, embedded at: $h = 2\,\text{cm}$. ΔS_{11} is obtained from the S_{11} measurement from these individual embedding dielectrics and one of the S_{11} obtained from D_1. As shown in Fig. 6, the normalized ΔS_{11} peaks are marked by asterisks "*" at around 2.35 GHz, 3.58 GHz and 4.85 GHz, denoting the resonant frequency f_r for inclusions of diameters 16, 12 and 8 mm respectively. Inclusions of different sizes resonate at different frequencies; the larger the inclusion, the lower the resonant frequency in the frequency scan of ΔS_{11}. To illustrate the possibility of using f_r to estimate size of inclusion, metal spheres of different sizes are used as the theoretical values of the first resonant frequency f_r of a perfect electrically conducting (PEC) sphere of diameter d_0 can be found from [20]

$$f_r \approx c \Big/ \pi d_0 \sqrt{\varepsilon_r'} \left[1 + \frac{1}{8}\left(\varepsilon_r''/\varepsilon_r'\right)^2\right] \tag{5}$$

where c is the speed of light in vacuum; and ε_r', ε_r'' are the real and imaginary parts of the relative complex permittivity of the nondispersive embedding medium. Hence the diameter of the inclusion can be estimated from the following expression

$$d_0 \approx c \Big/ \pi f_r^* \sqrt{\varepsilon_r'} \left[1 + \frac{1}{8}\left(\varepsilon_r''/\varepsilon_r'\right)^2\right] \tag{6}$$

where f_r^* is the observed resonant frequency.

At these observed f_r^* with $\varepsilon_r = 6(1 - j0.31)$ found by taking the average measured values of the 80% oil-concentration phantom over a scan from 1 to 6 GHz in Fig. 2, the predicted d_0 based on substituting into (6), $\varepsilon_r' = 6$, $\varepsilon_r''/\varepsilon_r' = 0.31$ and the f_r^* for the respective inclusions of 8 mm, 12 mm, and 16 mm are tabulated in the second column of Table 1. From Table 1, one observes that the error in the estimated and actual diameters of inclusions is less than about 10%. This shows the possibility of estimating the size of the inclusion from the calibrated resonant frequencies f_r. However this proposed technique can only estimate the size of the inclusion but not differentiate the shape of the inclusion, e.g., a spherical object from a spheroidal one.

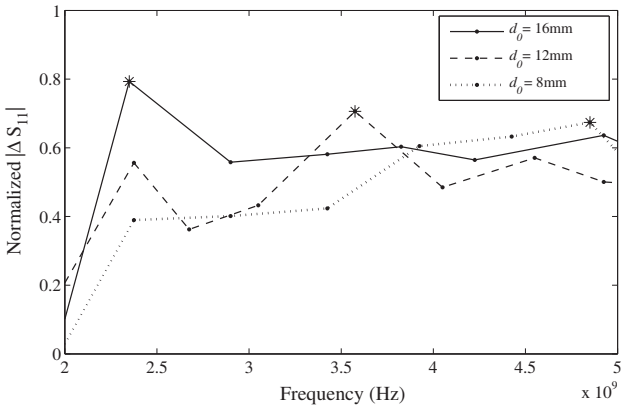

Figure 6. Normalised magnitude of ΔS_{11} for metal spheres of different diameters, embedded at a depth of 2 cm in the solid phantom.

Table 1. Comparison of diameter of inclusion embedded d_0 (mm).

f_r^* (GHz)	Calculated from (6)	Actual value	Percentage error
4.85	7.9	8	1.3
3.58	10.8	12	10.0
2.35	16.4	16	2.5

4.3.3. Effect of Clutters

We have also studied the influence of large homogeneities in the embedding medium by embedding clutter items (fabricated using 70% oil-concentration to give around 2 times the dielectric contrast from the embedding medium), on the detection of the targeted inclusion (fabricated using 10% oil-concentration to give around 8 times the dielectric contrast). The respective setups of the targeted inclusion and the clutter items are as depicted in Fig. 7. In the first setup, named as Setup 1, only the targeted inclusion and clutters '1' and '2' are present; whereas in Setup 2, only the inclusion and clutters '1', '2' and '3' are present; while in Setup 3, only the inclusion and clutters '1' to '4' are present. All the five clutters and one targeted inclusion as depicted in Fig. 7 are present in Setup 4. All spheres are of the same dimension, embedded at a depth of $h = 1.5\,\text{cm}$. It is observed in Fig. 8, for all setups, the backscattered signal from the 10% oil-concentration inclusion measured at position A (see Fig. 7) is the greatest over the swept frequencies. This further validates the previous concept in Section 3 that the PPDW can scan about the region of concern for maximum response in ΔS_{11} to locate the position underneath the PPDW where the targeted inclusion is embedded even under the influence of clutter items (inhomogeneities). As compared to the ΔS_{11} for the case where only the targeted inclusion but no clutters are present, there exists a slight shift in resonant frequencies and difference in amplitude in ΔS_{11} at position A for the setups. The shift in resonating frequencies may be attributed to the slight difference in sizes of the 10% oil-concentration inclusion used in all the 5 moulds fabricated (Setups '1' to '4' and another mould with only the targeted

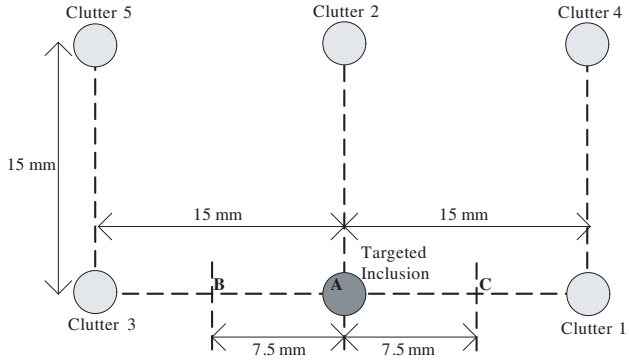

Figure 7. Top view of one type of configuration of the targeted inclusion and clutter items, embedded in the same phantom.

inclusion present) and the slight variation in dielectric properties in the separately fabricated phantoms. These complicate the qualitative attempt to analyze the effect of interferences contributed from the clutters with the backscattering from the tumor.

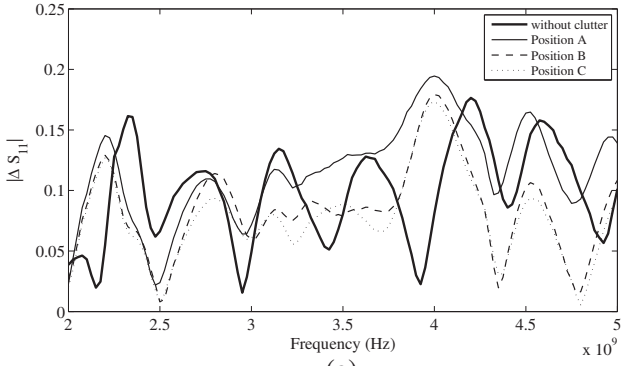

(a)

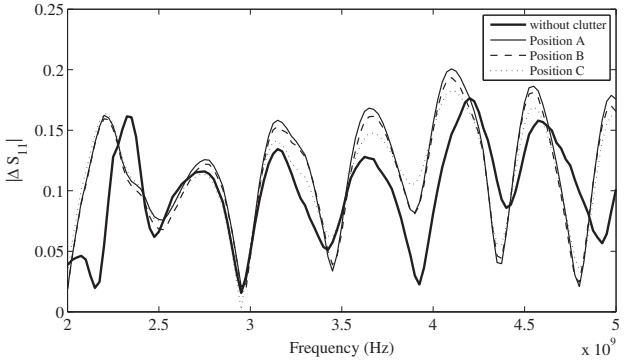

(b)

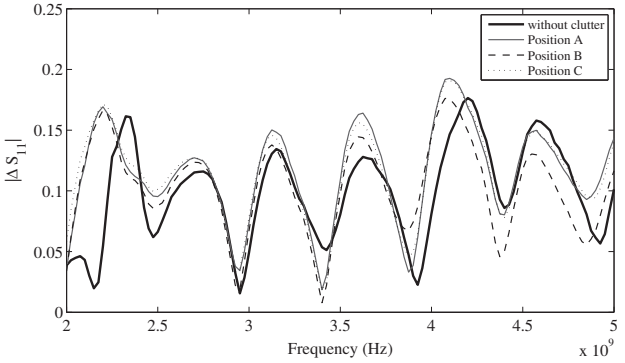

(c)

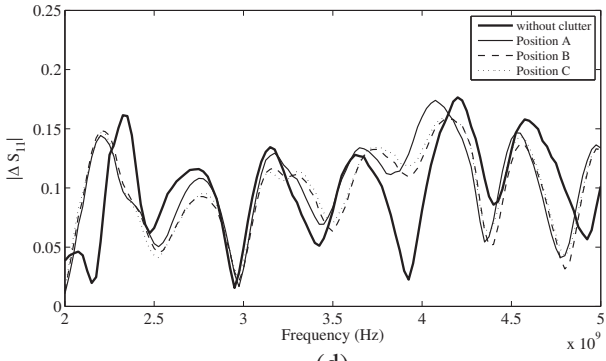

(d)

Figure 8. Magnitude of ΔS_{11} for an 8 mm dielectric sphere of 10% oil-concentration in the presence of clutter items. (a) Setup 1. (b) Setup 2. (c) Setup 3. (d) Setup 4.

5. CONCLUSION

This paper reports results of a study on the performance of a flanged parallel-plate dielectric waveguide probe (PPDW) for the detection and estimation of the sizes of buried targets that exhibit significant dielectric contrast from the embedding medium. This technique gives good results for cases where the buried inclusions have high dielectric contrast of about 8 times from the host medium. In principle, these buried inclusions need not be spherical although non-spherical inclusions would result in more complex calculations. The advantages of this waveguide probe for detection of buried objects are (1) simplicity of design, (2) ease of fabrication, (3) scalability, (4) ability to shape the source radiation pattern, and (5) ability to operate in a single mode over a wide frequency range. This technique may also be useful for detecting foreign objects in food products such as powdered milk, flour, rice and grains.

REFERENCES

1. Mahmoudi, M. and S. Y. Tan, "Depth detection of conducting marine mines via eddy-current and current-channeling response," *Progress In Electromagnetic Research*, Vol. 90, 287–307, 2009.
2. Ji, W.-J. and C.-M. Tong, "Bistatic scattering from two-dimensional dielectric ocean rough surface with a PEC object partially embedded by using the G-smcg method," *Progress In Electromagnetics Research*, Vol. 105, 119–139, 2010.
3. Huang, C.-W. and K.-C. Lee, "Application of ica technique to

PCA based radar target recognition," *Progress In Electromagnetics Research*, Vol. 105, 157–170, 2010.

4. Atteia, G. E. and K. F. A. Hussein, "Realistic model of dispersive soils using plrc-FDTD with applications to GPR systems," *Progress In Electromagnetics Research B*, Vol. 26, 335–359, 2010.
5. Lu, T., K. Agarwal, Y. Zhong, and X. Chen, "Through-wall imaging: Application of subspace-based optimization method," *Progress In Electromagnetics Research*, Vol. 102, 351–366, 2010.
6. Hajihashemi, M. R. and M. El-Shenawee, "The level set shape reconstruction algorithm applied to 2D PEC targets hidden behind a wall," *Progress In Electromagnetics Research B*, Vol. 25, 131–154, 2010.
7. Narayanan, R. M., M. C. Shastry, P.-H. Chen, and M. Levi, "Through-the-wall detection of stationary human targets using doppler radar," *Progress In Electromagnetics Research B*, Vol. 20, 147–166, 2010.
8. Soldovieri, F., A. Brancaccio, G. Prisco, G. Leone, and R. Pierri, "A Kirchhoff-based shape reconstruction algorithm for the multimonostatic configuration: The realistic case of buried pipes," *IEEE Trans. GeoSci. Remote Sensing*, Vol. 46, No. 10, 3031–3038, 2008.
9. Xu, P., K.-S. Chen, and L. Tsang, "Analysis of microwave emission of exponentially correlated rough soil surfaces from 1.4 GHz to 36.5 GHz," *Progress In Electromagnetics Research*, Vol. 108, 205–219, 2010.
10. Prakash, R., D. Singh, and N. P. Pathak, "The effect of soil texture in soil moisture retrieval for specular scattering at C-band," *Progress In Electromagnetics Research*, Vol. 108, 177–204, 2010.
11. Butnor, J. R., M. L Pruyn, D. C. Shaw, M. E. Harmon, A. N. Mucciardi, and M. G. Ryan, "Detecting defects in conifers with ground penetrating radar: Applications and challenges," *Forest Pathology*, Vol. 39, No. 5, 309–322, 2009.
12. O'Halloran, M., M. Glavin, and E. Jones, "Rotating antenna microwave imaging system for breast cancer detection," *Progress In Electromagnetics Research*, Vol. 107, 203–217, 2010.
13. Conceição, R. C., M. O'Halloran, E. Jones, and M. Glavin, "Investigation of classifiers for early-stage breast cancer based on radar target signatures," *Progress In Electromagnetics Research*, Vol. 105, 295–311, 2010.
14. Conceição, R. C., M. O'Halloran, M. Glavin, and E. Jones,

"Support vector machines for the classification of early-stage breast cancer based on radar target signatures," *Progress In Electromagnetics Research B*, Vol. 23, 311–327, 2010.

15. Chen, G., Z. Zhao, Z. Nie, and Q. H. Liu, "Computational study of time reversal mirror technique for microwave-induced thermo-acoustic tomography," *Journal of Electromagnetic Waves and Applications*, Vol. 22, No. 16, 2191–2204, 2008.
16. Davis, S. K., B. D. V. Veen, S. C. Hagness, and F. Kelcz, "Breast tumor characterization based on ultrawideband microwave backscatter," *IEEE Trans. Biomed. Eng.*, Vol. 66, No. 1, 237–246, 2008.
17. Pallav, P., G. G. Diamond, D. A. Hutchins, R. J. Green, and T. H. Gan, "A near-infrared technique for imaging food materials," *Journal Food Science,* Vol. 74, No. 1, E23–E33, 2009.
18. Zhang, H., S. Y. Tan, and H. S. Tan, "A novel method for breast cancer detection," *Progress In Electromagnetics Research*, Vol. 83, 413–434, 2008.
19. Zhang, H., S. Y. Tan, and H. S. Tan, "A flanged parallel-plate waveguide probe for microwave imaging of tumors," *Progress In Electromagnetics Research*, Vol. 97, 45–60, 2009.
20. Ruck, G. T., D. E. Barrick, W. D. Stuart, and C. K. Krichbaum, *Radar Cross Section Handbook*, Plenum Press, 1970.
21. Ang, T. W., S. Y. Tan, and H. S. Tan, "Analytical methods to determine diffraction points on multiple edges and cylindrical scatterers in UTD ray tracing," *Microw. Opt. Tech. Lett.*, Vol. 22, No. 5, 304–309, 1999.
22. Sun, Q., S. Y. Tan, and K. C. Teh, "Analytical formulae for path loss prediction in urban street-grid microcellular environments," *IEEE Trans. Veh. Tech.*, Vol. 54, No. 4, 1251–1258, 2005.
23. Lazabnik, M., E. L Madsen, G. R. Frank, and S. C. Hagness, "Tissue-mimicking phantom materials for narrowband and ultrawideband microwave applications," *Phys. Med. Biol.*, Vol. 50, 4245–4258, 2005.
24. Zhang, H., S. Y. Tan, and H. S. Tan, "Experimental study on flanged parallel-plate dielectric waveguide probe for early tumor detection," *Journal of Electromagnetic Waves Applications*, Vol. 24, No. 5–6, 681–693, 2010.
25. Zhang, H., S. Y. Tan, and H. S. Tan, "Microwave breast cancer detection via flanged parallel-plate dielectric waveguide probe," *Proceedings of International Conference on Electromagnetics in Advanced Applications*, 166–169, Torino, Italy, Sep. 2009.